Effects of MnO-Doping on the Structure of Sodium Metaphosphate Glasses

N. Zotov, H. Schlenz, B. Brendebach[a], H. Modrow[a], J. Hormes[a, b], F. Reinauer[c], R. Glaum[c], A. Kirfel, and C. Paulmann[d]

Mineralogisch-Petrologisches Institut, Universität Bonn,
Poppelsdorfer Schloss, D-53115 Bonn, Germany
[a] Physikalisches Institut, Universität Bonn, D-53115 Bonn, Germany
[b] Center for Advanced Microstructures and Devices, 70806 Baton Rouge, LA, U. S. A.
[c] Institut für Anorganische Chemie, Universität Bonn, D-53121 Bonn, Germany
[d] Mineralogisch-Petrologisches Institut, Universität Hamburg, D-20146 Hamburg, Germany

Reprint requests to Dr. N. Z.; Email nzotov@uni-bonn.de; Fax: +49-228-732770

A combined structural study on ternary phosphate glasses $(MnO)_x(NaPO_3)_{1-x}$, $x = 0.0$, 0.024, 0.048, 0.167, is performed using X-ray diffraction, EXAFS and Raman spectroscopy. The mean Mn-O nearest-neighbour distance and the Mn-O coordination number in the glass with 16.7 mol% MnO are 2.15(2) Å and 5.7 ± 0.4, respectively. Depolymerization of the metaphosphate chains in the $NaPO_3$ glass structure is observed with increasing MnO content by Raman scattering. This leads to a strong decrease of the average chain length and a small decreasing of the average P-O-P bridging angle with increasing MnO content.

Key words: Phosphate Glasses; Transition Metals; X-ray Diffraction; Raman Spectroscopy; EXAFS.

1. Introduction

Bulk phosphate glasses containing a great variety of metal cations can be prepared by melt quenching or sol-gel methods. The structure of simple binary alkali and alkaline-earth as well as some multicomponent phosphate glasses has been summarized in several recent reviews [1 – 4].
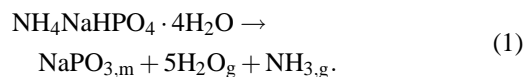
Transition metal oxides dissolve readily in phosphate glasses giving characteristic coloration [5, 6] which sensitively depends on the oxidation state and the coordination of the transition metal and arises mostly from d-d electronic transitions. However, very few studies on the structure and the physical properties of transition metal-doped alkali phosphate glasses have been performed so far [7 – 14].

In the present paper we report results on the structure of MnO-doped sodium metaphosphate glasses using a combination of X-ray diffraction, EXAFS and Raman spectroscopy in order to understand better the incorporation mechanisms of transition metals in phosphate glasses.

2. Experimental Procedures

2.1. Glass Preparation

The Mn-doped sodium metaphosphate glasses were prepared in two steps. In the first step, $NaPO_3$ melt was obtained by decomposition of $NH_4NaHPO_4.4H_2O$ p. a. (Merck, Darmstadt) in a gold crucible (~ 20 ml) at about 1023 K according to the reaction

$$NH_4NaHPO_4 \cdot 4H_2O \rightarrow \\ NaPO_{3,m} + 5H_2O_g + NH_{3,g}. \tag{1}$$

Because of the strong degasing of water and ammonia, the hydrogen phosphate was added into the crucible in small portions of about $1 - 2$ g. The melt was heated under occasional stiring with a magnesia skewer until no gaseous bubbles were observed.

In the second step, Mn_2O_3 oxide was added to the melt in small amounts of about 10 mg until all of the oxide was dissolved under constant stirring. The dissolution of Mn_2O_3 was accompanied by the formation of $O_{2,g}$ indicating reduction of Mn^{3+} to Mn^{2+} under

Table 1. Chemical composition (mol%) and density of the investigated glasses.

Sample	MnO*	NaPO₃*	Density (g/cm³)
MN0	0.0	100	2.37(12)
MN1	2.4	97.6	2.19(12)
MN2	4.8	95.2	2.05(10)
MN3	16.7	83.3	2.47(4)

* estimated error 0.1 mol%.

the given conditions. The melt was then annealed at 1073 K for four hours, poured on a Pt metal plate and pressed with a metal block, both cooled with liquid nitrogen. The glass plates obtained were then annealed at 373 K for at least four hours in a drying furnace. The pure $NaPO_3$ glass is colorless whereas the Mn-doped glasses have a violet color, typical for manganese(III)-containing phosphates [5]. However, Mn(III) titration analysis of the glass with the highest Mn content yielded only about 3% Mn^{3+} ions. Taking also into account the release of O_{2g} during the preparation, the composition of the quenched glasses is written as $(MnO)_x(NaPO_3)_{1-x}$. The chemical compositions of the quenched glasses were checked by ICP analysis and are given in Table 1 together with the respective density values. The density was measured picnometrically using extra pure toluene (Merck). Four glasses with $x = 0.0, 0.024, 0.048$ and 0.167 are studied, which will be denoted MN0, MN1, MN2 and MN3 hereafter. A minimum in the density is observed for the MN2 sample.

2.2. X-ray Diffraction

The X-ray diffraction experiments were performed at the F1 beamline at HASYLAB (DESY, Germany) in Debye-Scherrer geometry using a Si (111) double-crystal monochromator, $\lambda = 0.496$ Å and a vertical Huber diffractometer equipped with a scintillation detector. The detector slit was 0.8 mm. Measurements were done on the pure $NaPO_3$ glass and the MN3 sample, which is expected to show the largest diffraction difference from the pure $NaPO_3$ glass. The powdered samples were loaded in thin silica glass capillaries (1.0 mm diameter, 0.01 mm wall thickness) bathing in the primary beam. The two samples and an empty capillary were measured 6 times from 3° to 140° 2Θ with a step 0.05° 2Θ and 5 s/step counting time. The effective linear absorption coefficient μ was determined experimentally from transmission experiments. Each data set was first corrected for the decay of the ring current using the primary-beam monitor data, and ex-

cellent internal agreement between the different runs for each sample was obtained. The six measurements for each sample were then averaged, the standard deviations of the mean, $\sigma_m(I)$, were calculated at each 2Θ point and used in the subsequent error propagation analysis as a measure of the experimental uncertainties. The averaged curve for the MN0 sample was additionally Fourier-smoothed.

The intensities were then corrected for background scattering, detector dead time (approximately 6 μs), absorption in the sample (using the measured μR coefficients and the method of Sabine et al. [15]), polarization of the incident beam (vertical polarization fraction 0.9) and Compton scattering. In principle, an analyser crystal with a narrow energy band-pass could be used to remove part of the Compton scattering at large scattering angles. But at low scattering angles the elastic coherent and the inelastic incoherent scattering overlap strongly in energy and cannot in practice be separated in this fashion. Recently, a new procedure for seperation of the Compton scattering using a dispersive X-ray technique was proposed [16], but such experimental setup is not available at the F1 beamline. That is why the Compton scattering was calculated using the analytical approximation to the incoherent X-ray scattering intensities published by Balyuzi et al. [17] and the full Klein-Nishina formula [18]. The corrected total scattering was then normalized to the sum of the independent scattering $\langle f^2 \rangle$ and the calculated Compton scattering using both the Krogh-Moe [19] and the high-Q method (where $Q = 4\pi \sin(\Theta)/\lambda$). The normalization constants derived from the two methods are in good agreement (differences less than 2%) for both samples, thus giving confidence in the consistence of our correction procedures. Similar Compton correction and normalization procedures have been used in all other recent X-ray diffraction studies of phosphate glasses carried out at synchrotron sources with photon energies ≥ 25 keV [20–24].

The reduced pair-correlation functions $G(r)$ were calculated as the Fourier transforms of the interference functions, $i(Q) = (I_{coh}(Q) - \langle f^2 \rangle)/\langle f \rangle^2$, where $I_{coh}(Q)$ is the corrected normalized coherent scattering. Taking into account the level of the statistical noise, the reduced interference functions, $Qi(Q)$, have been smoothed for $Q > 13$ Å^{-1}. The mean and mean-square scattering functions, $\langle f \rangle$ and $\langle f^2 \rangle$, were calculated using analytical expressions for neutral atoms [25] taking into account the anomalous dispersion corrections. The total pair correlation functions, $T(r) = 4\pi\rho_o r$

+ $G(r)$, where ρ_o is the atom number density, were corrected for small residual errors at high-Q following the method of Kaplow, Averbach and Strong [26]. A Lorch modification function [27], $\sin(\alpha Q)/\alpha Q$, with $\alpha = 0.132$, was also used to downweight the termination ripples caused by the finite Q-range.

2.3. Raman Spectroscopy

Raman spectra (both unpolarized and polarized) were measured for all compositions using a BRUKER FTIR Raman spectrometer in backscattering (180°) geometry and a YAG laser with $\lambda = 1036$ nm wavelength. The laser power was 0.4 W. Measurements were done on flat bulk pieces. The frequency calibration was checked before and after the measurements using a crystalline Si wafer. The unpolarized measurements were performed with $2\,\mathrm{cm}^{-1}$ resolution accumulating 120 scans per sample. The polarized measurements were performed using a polarizer in the scattered beam, $4\,\mathrm{cm}^{-1}$ resolution and accumulating from 64 to 1024 scans per sample. The accuracy in the depolarization ratio ($\pm 10\%$) was determiend by recording the A_1 line of CCl_4 at $460\,\mathrm{cm}^{-1}$.

2.4. EXAFS Measurements

Mn K-edge EXAFS experiments were carried out at the beamline BN3 of the Electron Stretcher Accelerator ELSA (operating at 2.3 GeV energy) [28] using a modified Lemmonier-type double-crystal monochromator with a set of Ge (220) crystals [29, 30]. The measurements were performed in transmission mode at ambient conditions for the MN3 sample (16.7 mol% MnO) which is expected to give the strongest EXAFS signal from the Mn-P partial pair correlations. The grounded sample was fixed between two layers of self-adhesive Kapton tape. The thickness of the sample was optimized to result in an edge jump of approximately 1 atomic unit. Spectra were recorded at least three times and then averaged. Crystalline MnO, used as a standard, was measured under the same conditions. The ion currents, measured with ionization chambers operating at 200 V, were read out using Balzers QME 311 electrometers. The spectra were measured from 6350 to 7550 eV in steps of 1.2 eV and 400 ms integration time per step. The spectrum of Mn powder, whose first inflection point was set to an energy of 6539 eV, was recorded before and after each scan in order to achieve best possible energy calibration. The absorption spec-

tra μt were calculated from the logarithmic ratio of the detector- and monitor-currents according to Lambert-Beer's Law. The EXAFS spectra were extracted from the measured absorption spectra by a linear fit in the pre-edge region and by cubic spline functions in the after-edge region. The UWXAFS [31] and FEFF7 [32] suites of programs were used for data processing and analysis.

3. Results

3.1. X-ray Diffraction

The coherent scattering curves $I_{\mathrm{coh}}(Q)$ and $\langle f^2 \rangle$ for the MN0 and the MN3 samples are shown in Figure 1. The standard deviations, $\sigma(I_{\mathrm{coh}}(Q))$, given for clarity in Fig. 1 only at selected Q-values, were calculated on the basis of the mean standard deviations of the sample and the background scattering intensites by error-propagation analysis [33]. The coherent scattering curve for the pure $NaPO_3$ glass is compared with previous data [34] in the inset of Fig. 1a, showing good quantitative agreement.

The corresponding total pair-correlation functions, $T(r)$, are shown in Figure 2. The inset in Fig. 2 shows $T(r)$ for the pure $NaPO_3$ glass with and without the Kaplow, Averbach, and Strong correction [26]. The average nearest-neighbour P-O, O-O and P-P distances in crystalline $NaPO_3$ (Kurrol salt type A) [35] are 1.54(1) Å, 2.57(7) Å and 2.91(4) Å, respectively. Therefore, the peaks at about 1.5 Å, 2.5 Å and 2.9 Å in $T(r)$ of the MN0 glass can be attributed to the P-O, O-O and P-P average nearest-neighbour distances in the glass structure. These assignments are in full agreement with previous diffraction results [4, 9, 34, 36], reverse Monte Carlo [34] and molecular dynamics [37] simulations of the pure $NaPO_3$ glass.

Qualitative comparison of the peak positions in the $T(r)$ functions of the MN0 and MN3 samples shows that the addition of MnO does practically not affect the mean nearest-neighbour P-O, O-O and P-P distances. However, the peaks in the experimental $T(r)$ represent convolutions of the actual partial pair correlation functions $g_{ij}(r)$ with the corresponding shape functions $Q_{ij}(r)$ [38]. That is why, in order to quantitatively determine the effect of MnO on the P-O coordination number and bond-length variations, we have fitted the P-O peaks in the $T(r)$ functions by a convolution of a single Gaussian function with the corresponding P-O shape function (Figure 3). Although the distances from
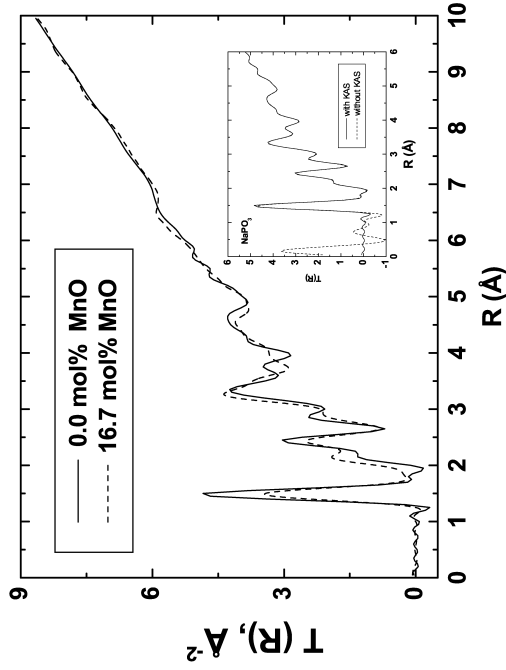
Fig. 2. Total pair correlation functions $T(r)$: NaPO$_3$ glass (full line), (MnO)$_{0.167}$ (NaPO$_3$)$_{0.833}$ glass (dashed line). The inset shows $T(r)$ of the NaPO$_3$ glass with (full line) and without (dotted line) the KAS correction [26].
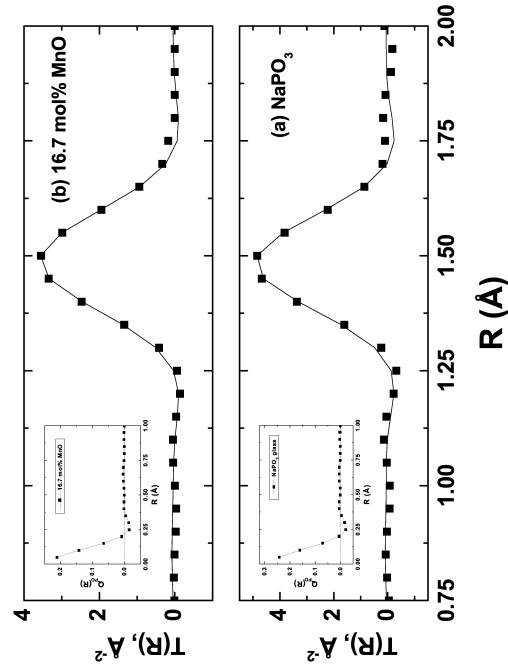

Fig. 3. Fit of the pair-correlation functions $T(r)$ in the range $0.75-2.0$ Å: (a) NaPO$_3$ glass; (b) (MnO)$_{0.167}$(NaPO$_3$)$_{0.833}$ glass. Exp. points (■), fit (full line). The insets show the corresponding shape functions $Q_{PO}(r)$.
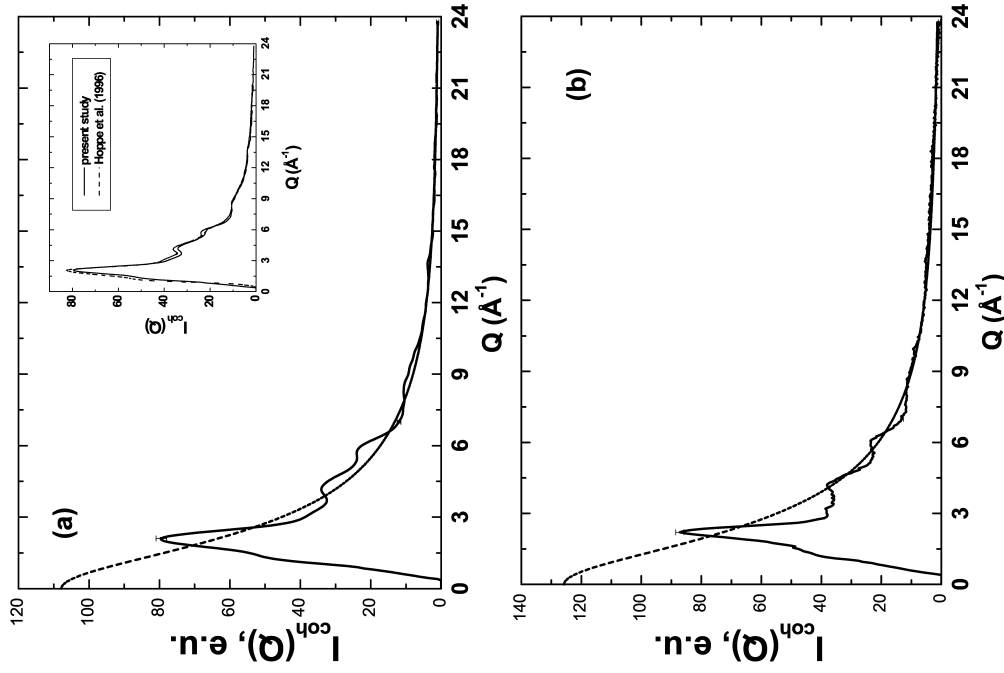

Fig. 1. Coherent scattering intensities for: (a) NaPO$_3$ glass, (b) (MnO)$_{0.167}$(NaPO$_3$)$_{0.833}$ glass. Experimental points (full line), mean-square scattering curve $\langle f^2 \rangle$ (dashed line). The inset in (a) shows the coherent scattering intensities of the NaPO$_3$ glass from the present study (full line) and from Hoppe et al. [34] (dashed line).

the bridging oxygen (BO) and from the non-bridging oxygen (NBO) atoms to the central P atom are known to be different [4, 26, 39], only one Gaussian function was used, becasue the real-space resolution of the experiments is not sufficient to separate them. The fits confirm that the average P-O distance remains practically the same ($\sim$ 1.51(1) Å) upon addition of MnO. The P-O coordination, determined from the area under the P-O peak in the total radial distribution functions $RDF(r) = rT(r)$, also does not change: 3.8(2) in the pure NaPO$_3$ glass and 4.0(1) in the MN3 glass. However, adding MnO leads to a slight increase of the P-O bond-length variation as revealed by the full widths at half maximum: 0.136(3) Å in the pure NaPO$_3$ glass and 0.159(1) Å in the MN3 glass.

The second peak in the $T(r)$ function of the MN3 sample at about 2.5 Å contains contributions from three partial pair correlations (Mn-O, Na-O and O-O). Fitting of the $T(r)$ function in this range was not attempted because the actual shapes of these distributions are not exactly known and the real-space resolution of the experiment is not sufficient to separate them.

The significant intensity *increase* of the shoulder at about 2.15 Å in the $T(r)$ function of the MN3 sample gives, however, a direct indication for the presence of Mn-O distances of about 2.15 Å in the MN3 glass structure. This value is in general agreement with the Mn-O nearest-neighbour distance of about 2.20(5) Å, reported by Cervinka et al. [40] for pure Mn(PO$_3$)$_2$ glass. Similarly, we observe some increase in the intensity of the $T(r)$ peak of the MN3 sample at about 3.25 Å.

3.2. EXAFS Spectroscopy

Several EXAFS studies of metal-doped phosphate glasses can be found in recent publications, most of which are devoted to rare earth elements [41 – 44] or transition metals (Ni, Fe, Cu, Zn) [45 – 49]. To the best of our knowledge the present work is the first Mn K EXAFS study of Mn-doped metaphosphate glasses.

The k^3-weighted $\chi(k)$ EXAFS spectra of the MN3 sample and the MnO crystalline standard are shown in Figure 4. The k^3-weighted EXAFS spectra were Fourier transformed in the photoelectron wavevector range $2.5 \leq k \leq 13.2$ Å^{-1} for the MnO standard and in the $2.5 \leq k \leq 10$ Å^{-1} range for the MN3 sample using a 2Å^{-1} Hanning window. The Fourier transforms (FTs) are given in Figure 5. Both EXAFS radial distribution functions exhibit Mn-O first-shell correlations
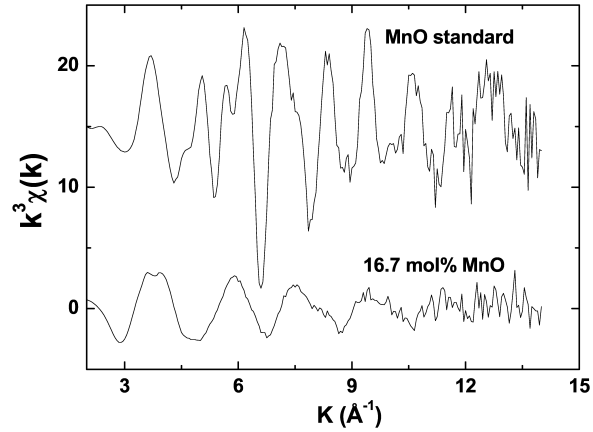
Fig. 4. k^3-weighted EXAFS spectra $\chi(k)$ of the MnO standard and the MN3 glass sample. The MnO curve is shifted along the y axis for clarity.
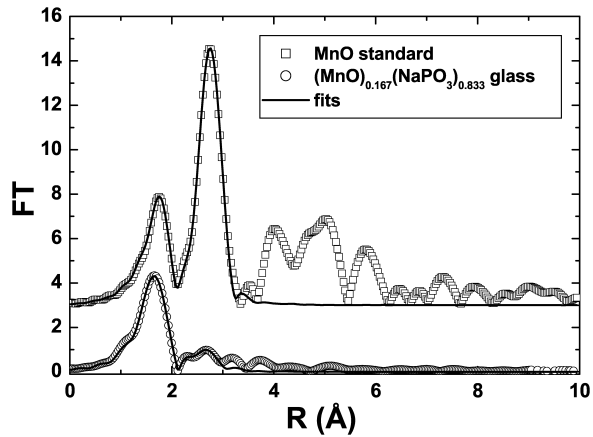
Fig. 5. Experimental Fourier-transformed EXAFS spectra of the MnO standard (□) and the MN3 glass sample (*circle*) together with fits of the first and the second shells (full lines). The MnO spectra are shifted along the y axis for clarity.

with peaks centered at about 1.65 Å. In the EXAFS spectrum of the MnO standard the strongest peak at about 2.7 Å is due to Mn-Mn distances in the second coordination sphere.

In order to determine the average distances and coordination numbers the multi-shell formula in the plane-wave approximation [50] has been applied:

$$\chi(k) = S_o^2 \Sigma_i (N_i/kR_i^2) f_i(k) \exp(-2\sigma_i^2 k^2)$$
$$\cdot \exp(-2R_i/\lambda_i(k)) \sin(2kR_i + \phi_i(k)), \qquad (2)$$

where $k = ((2m/\hbar^2)(E - E_0 - \Delta E_o))^{1/2}$ is the photoelectron wavevector, ΔE_o is the E_o correction, N_i and
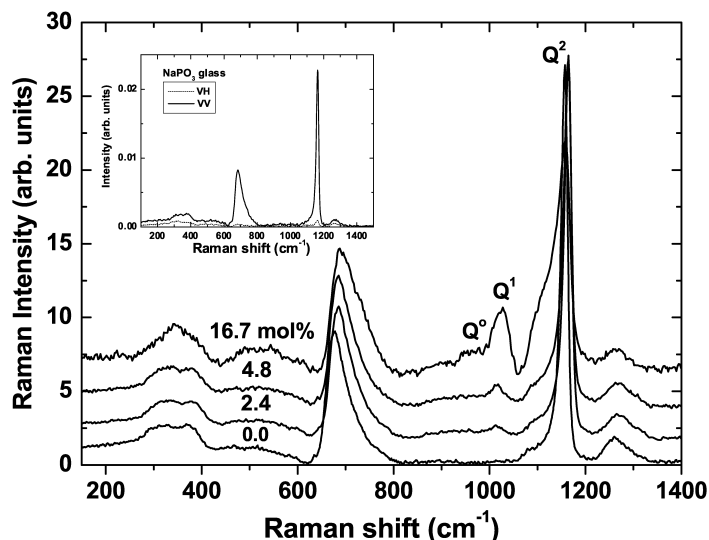
Fig. 6. Unpolarized Raman spectra of the investigated glasses. The spectra are background corrected and scaled to have the same peak intensity at about 685 cm^{-1}. The spectra for the samples with 2.4, 4.8 and 16.7 mol% MnO are shifted along the *y* axis (from bottom to top) for clarity. The inset shows the polarized spectra for the NaPO$_3$ glass: VV polarization (full line), VH polarization (dotted line).

R_i are the coordination number and the mean absorber-scatterer distance in the ith shell, σ_i is the corresponding Debye-Waller factor, $\lambda(k)$ the electron incoherent mean-free path and S_o^2 the amplitude reduction factor.

The first-shell and the second-shell peaks in the 1.2 – 3.3 Å range of the EXAFS spectrum of the MnO standard have been fitted in real space using (2) and the least-squares fitting routine of the UWXAFS package [31] which takes into account the presence of residual background oscillations. The amplitude factors, the phase-shifts and the electron mean-free paths for the first-shell Mn-O and the second-shell Mn-Mn peaks were determined by the FEFF7 [32] program. The Mn-O and the Mn-Mn distances were kept fixed at the respective values, 2.2 Å and 3.144 Å in the MnO crystal structure [51]. Similarly, the Mn-O and the Mn-Mn coordination numbers (6 and 12, respectively) were kept fixed while the amplitude factor S_o^2, the corresponding rms displacements and the ΔE_o values were refined in order to obtain best possible fits of the experimental data. The refined S_o^2 value is equal to 0.62(2). This value is close to the value 0.7, employed in other EXAFS studies of metaphosphate glasses [41 – 42], and was used without adjustments in the fit of the MN3 glass data. Preliminary fits of the second-shell peak in the EXAFS spectrum of the MN3 sample at about 2.6 Å indicated that it is due to Mn-P correlations. Hence, the Mn-P amplitude factors, phase-shifts and the electron mean-free path were calculated using the crystallographic data for the Mn$_2$P$_2$O$_7$ structure [52] and the FEFF7 [32] program, while the Mn-O ampli-

tude factors, phase-shifts and electron mean-free paths were the same used in the MnO fit. Then, the first- and the second-shell peaks in the Fourier transformed EXAFS spectrum of the MN3 sample were fitted in the range 1.2 – 3.0 Å using (2).

The fits of the first- and the second shell are shown in Figure 5. The avearge Mn-O nearest-neighbour distance in the MN3 glass is 2.15(2) Å, the Mn-O coordination number is 5.7(4) and the rms displacement parameter σ_{Mn-O}^2 is 0.010(1) Å^2. The average Mn-P distance is 3.26(2) Å, the Mn-P coordination number is 4.1(1.9) and σ_{Mn-P}^2 is 0.016(5) Å^2. Thus, the mean Mn-O nearest-neighbour distance, derived from the EXAFS data agrees well with the position of the Mn-O peak in the total pair correlation function $T(r)$, determined by X-ray diffraction.

3.3. Raman Spectroscopy

The unpolarized Raman spectra of all investigated glasses are shown in Figure 6. All spectra show: (i) weak partially depolarized low-frequency bands at about 316, 382 and 500 cm^{-1} (for clarity in Fig. 6 the only polarized Raman spectra for the NaPO$_3$ glass are shown). In the MN3 sample the 316 and 382 cm^{-1} peaks merge. (ii) a strong asymmetric polarized band (depolarization ratio $\rho \sim 0.05$) at about 700 cm^{-1}; (iii) a very strong polarized band ($\rho = 0.05 - 0.1$) at about 1164 cm^{-1} with a shoulder at about 1100 cm^{-1} and (iv) a medium-intensity depolarized band ($\rho \sim 0.5$) at about 1274 cm^{-1}.
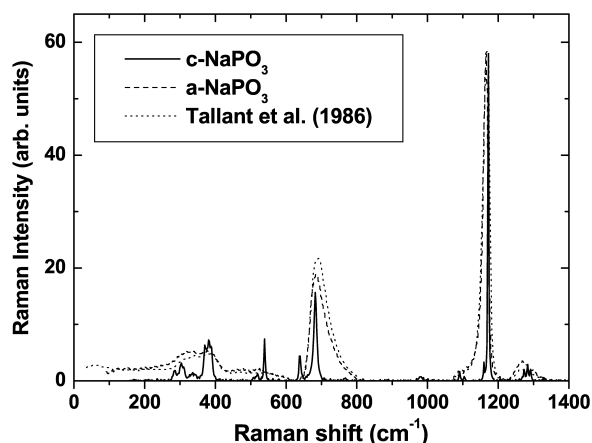
Fig. 7. Unpolarized Raman spectra of crystalline $NaPO_3$ (full line), $NaPO_3$ glass from the present study (dashed line) and from [53] (dotted line).

The unpolarized Raman spectrum of the pure $NaPO_3$ glass is compared in Fig. 7 with previous Raman data [53] and with the unpolarized Raman spectrum of crystalline $NaPO_3$ measured under the same conditions. Good agreement with previous measurements is observed [53 – 58]. The Raman spectrum of the $NaPO_3$ glass is essentially an envelope of the Raman spectrum of crystalline $NaPO_3$. Since similar observations are made for other alkali phosphate glasses [59] they provide evidence that the structure of alkali metaphosphate glasses is mainly built of long phosphate chains linked by M-O-M interactions (M=Na, K, etc). Correspondingly, the vibrational spectra are qualitatively interpreted in terms of the vibrations of the polyphosphate backbone chains [1].

The depolarized Raman band at about 1274 cm^{-1} is assigned to the asymmetric stretching vibrations of the non-bridging oxygens (NBO) against the P atoms. Since there are on average 2 NBO per P atom in the $NaPO_3$ structure, this vibration is usually denoted $v_{as}(PO_2)$. Likewise, the strongly polarized band at about 1164 cm^{-1} is assigned to the symmetric stretching vibrations of the NBO against the P atoms ($v_s(PO_2)$). The $v_s(PO_2)$ band is asymmetrically broadened towards lower frequencies and the asymmetry increases with increasing MnO content. The strongly polarized band at about 685 cm^{-1} is assigned to the symmetric in-plane bending vibration, v_s(P-O-P), of the bridging oxygens connecting two PO_4 tetrahedra. Bues and Gehrke [54] assigned the bands in the range 250 – 350 cm^{-1} in the spectrum of pure $NaPO_3$ glass to bending vibrations. On the other hand, Rouse et al. [56]

assigned the bands at about 212 cm^{-1} and 380 cm^{-1} to Na-O stretching and O-P-O bending vibrations, respectively. These assignment are still in question and will not be considered further.

A small increase of the average v_s(P-O-P) frequency is observed with increasing MnO content. This effect can be attributed to a decrease of the average P-O-P bond angle. The average P-O-P bond angle decreases from 130° in crystalline $NaPO_3$ (Kurrol salt type A) [35] to 127.5° in crystalline $Na_4P_2O_7$ [60]. Correspondingly, the v_s(P-O-P) frequency increases from 682 cm^{-1} in crystalline $NaPO_3$ to 731 cm^{-1} in crystalline $Na_4P_2O_7$ which was measured under the same conditions. Using these band positions of the v_s(P-O-P) vibration in crystalline $NaPO_3$ and $Na_4P_2O_7$, we have constructed a linear calibration curve for the P-O-P bond angle as a function of the v_s(P-O-P) frequency. A similar correlation between the P-O-P bond angle and the v_s(P-O-P) frequency has been proposed for crystalline pyrophosphates [61]. The average P-O-P bond angle in the $NaPO_3$ glass calculated from this calibration line is 129.3(2)°, which slightly decreases to 128.8(3)° in the MN3 sample. The average P-O-P bond angle determined for the $NaPO_3$ glass (129.3°) agrees well with the value 130° determined from high-resolution neutron diffraction [39].

With increasing MnO content we observe in the MN1 and MN2 samples some increase of the overall background in the range 850 – 950 cm^{-1} and the development of a new polarized Raman band (polarization ratio $\sim 0.1 – 0.2$) at about 1020 cm^{-1}. This band is usually assigned to the symmetric stretching vibration of the NBOs against the P atoms in PO_4 tetrahedra with 3 NBOs [1, 8, 55, 62, 63]. In the Raman spectra of the MN3 sample a weak band at about 964 cm^{-1} is also observed. It is usually assigned [1, 55] to the symmetric stretching vibrations of isolated $[PO_4]^{3-}$ tetrahedra. In other words, the Raman spectra show that the addition of MnO leads to a *depolymerization* of the structure of the $NaPO_3$ glass.

In order to quantitatively determine the depolymerization effect of MnO we have calculated the amount of Q^2-, Q^1- and Q^0-species using the unpolarized Raman spectra, where Q^n denotes PO_4 tetrahedra with n bridging oxygens. In principle ^{31}P MAS NMR is the best method for determining the Q-species distribution in phosphate glasses [1, 11] but the presence of MnO in the investigated glasses precludes the use of the NMR technique. The areas under the peaks at about 1020 cm^{-1} (Q^1-species) and at about 1164 cm^{-1} (Q^2-

Table 2. Distribution of the different Q-species (%) in $(MnO)_x(NaPO_3)_{1-x}$ glasses as determined by Raman spectroscopy (Rs) and from the chemical composition (Cc).

Mol% MnO	Q^0 Rs	Q^1 Rs	Cc*	Q^2 Rs	Cc**
0.0	0.0	0.0	0.0	100.0	100.0
2.4	0.0	2.0	5.0	98.0	95.0
4.8	0.0	4.0	10.0	96.0	90.0
16.7	10.0	15.0	40.0	75.0	60.0

* $c(Q^1) = 100 - c(Q^2)$.   ** using (3).

species) were numerically integrated. The integration limits were 975 cm^{-1} – 1050 cm^{-1} for the first peak and 1060 cm^{-1} – 1220 cm^{-1} for the second peak. In the MN3 sample, however, the Q^1-peak overlaps the Q^0-peak (Fig. 6). Therefore, the Q^0- and the Q^1-peaks were separated in this case by Gaussian fitting. Assuming that all Q-species have equal Raman scattering cross-sections which are independent of the MnO content, the concentrations of the Q^2-, Q^1- and Q^0-species given in Table 2 were calculated using the corresponding integrated intensities.

In order to check the assumption of equal, composition-independent scattering cross-sections, we have also calculated the percentage of the Q^2-species (see Table 2) using a modification of the formula proposed by Van Wazer [64]:

$$c(Q^2) = 100*(2 - R), \tag{3}$$

where $R = ([MnO] + [Na_2O])/[P_2O_5]$, and [MnO], [Na$_2$O] and [P$_2O_5$] are the mol% of the corresponding oxides.

The data in Table 2 quantitatively show that the addition of MnO leads to a depolymerization of the metaphosphate chains. As a result, the concentration of the infinite $[PO_3]_\infty^-$ chains (Q^2-species) decreases at the expense of finite chains possessing Q^1-end groups and isolated Q^0 groups in the MN3 sample. The concentration of the Q^1-species, calculated by both methods, increases linearly with the MnO content. This shows that the Raman scattering cross-sections are practically independent of the MnO concentration. However, the comparison between the results of the two methods indicates that the Raman scattering cross-sections of the Q^1- and Q^2-species are probably not equal, and thus only a qualitative discussion of the changes in the Q-species distribution on the basis of the Raman spectra of the investigated ternary phosphate glasses is possible without independent information about the Raman scattering cross-sections.

4. Discussion

4.1. Mn Coordination

Both the X-ray diffraction and the EXAFS results show that the mean Mn-O bond length in the MN3 sample is 2.15(2) Å. The EXAFS measurements yield an Mn coordination number of 5.7 ± 0.4 oxygen atoms in the MN3 glass. In order to rationalize these results a number of Mn-containing oxide, phosphate and fluoride structures contained in the inorganic structures data base ICSD [65] were analysed. In the majority of the Mn^{2+}-, Mn^{3+}- and Mn^{4+}-containing phases, Mn is 6-coordinated. The average Mn^{2+}-O distance for 6-coordinated Mn^{2+} is 2.20(4) Å. There are only a few inorganic structures in which Mn^{2+} is 4-coordinated with an average Mn^{2+}-O distance of 2.04(6) Å. Comparing the value 2.15(2) Å, found in the MN3 glass, with the mean Mn-O distances for 6- and 4-coordinated Mn(II), one can conclude that Mn is in a mixed-coordination state in the MN3 sample. Assuming that Mn^{2+} in the investigated glass is either 6-coordinated (with concentration c_6) or 4-coordinated (with concentration c_4) implies that $c_4 + c_6 = 1$ and $2.04c_4 + 2.20c_6 = 2.15$. From these two constraints we obtain that there should be about 31.2% 4-coordinated Mn^{2+} and 68.8% 6-coordinated Mn^{2+} in the MN3 sample. This result corresponds to an average Mn-O coordination number of about 5.4, in good agreement with the coordination number 5.7(4) directly determined from EXAFS.

4.2. Chain Lengths

The increase in the concentration of the Q^1-species at the expense of the Q^2-species (see Table 2) indicates the formation of finite phosphate chains. Variations in the P-NBO nearest-neighbour distances in chains with different lengths are most likely the reason for: (i) the observed increase of the FWHM of the P-O peak in the $T(r)$ functions and (ii) the asymmetry of the 1164 cm^{-1} Raman band.

A variety of spectroscopic methods (XPS, P L-edge XANES, ^{31}P NMR) can detect changes in the distribution of polyphosphate chain lengths [3, 66, 67]. The distribution of chain lengths is best determined by high-resolution chromatography [3, 68, 69], but this technique can quantitatively detect only phosphate chain with lengths up to about 30 – 50 tetrahedra [3].

In the present study the average chain length L_{ch}, defined as the number of P atoms in the chain, was calculated by an expression proposed by Van Wazer [64]:

$$(1/L_{ch}) = (R - 1)/2, \qquad (4)$$

where R is the molar ratio defined in (3).

The average chain lengths, calculated from (4), are 40, 20 and 5 tetraheda for the MN1, MN2 and MN3 samples, respectively. These values show that the addition of 16.7 mol% MnO leads to a strong decrease of the infinite phosphate chain length in the pure $NaPO_3$ glass to $L_{ch} = 5$ in the MN3 sample. This effect was also observed in binary copper phosphate glasses $(CuO)_x(P_2O_5)_{(1-x)}$ [70] with increasing CuO content. Comparing the shape and the FWHM of the $v_s(POP)$ vibration at about 685 cm^{-1} (Fig. 6) with the average chain lengths given above, it can be seen that the substantial decrease of the average chain length has practically no affect on the P-O-P bond-angle distribution. Thus, the addition of MnO to the $NaPO_3$ glass leads mainly to shortening of the metaphosphate chains rather than to stretching (compressing) of the chains, because the latter effect would lead to changes in the P-O-P bond-angle distribution and correspondingly in the shape of the $v_s(POP)$ vibration.

5. Conclusions

The structure of MnO-doped $NaPO_3$ glasses has been studied by X-ray diffraction, EXAFS and Raman spectroscopy in order to determine the Mn environment and the effects of MnO doping on the short- and medium-range order in the $NaPO_3$ glass structure.

The addition of MnO has practically no influence on the mean P-O bond-length of the PO_4 tetrahedra. However, it leads to an increase of the P-NBO bond-length variations and a small decrease of the average P-O-P bond angle.

Analysis of the EXAFS data for the $(MnO)_{0.167}$ $(NaPO_3)_{0.833}$ sample yields an average Mn-O distance of 2.15(2) Å and an Mn-O coordination number equal to 5.7 ± 0.4. The mean Mn-P distance is 3.25(2) Å and the mean Mn-P coordination number is 4.1 (1.9).

The most pronounced effect of the addition of MnO is a depolymerization of the $NaPO_3$ glass structure. The concentration of long but finite phosphate chains (Q^1-species) increases at the expense of the infinite metaphosphate chains (Q^2-species).

[1] S. W. Martin, Eur. J. Solid State Inorg. Chem. **28**, 163 (1991).

[2] U. Hoppe, J. Non-Cryst. Solids **195**, 138 (1996).

[3] R. K. Brow, J. Non-Cryst. Solids **263-264**, 1 (2000).

[4] U. Hoppe, G. Walter, R. Kranold, and D. Stachel, J. Non-Cryst. Solids **263 – 264**, 29 (2000).

[5] G. Ackerman, Z. Anorg. Chem. **323**, 149 (1963).

[6] W. A. Weyl, Colour of Glasses, Society of Glass Technology, 1951.

[7] P. H. Gaskell, J. Zhao, P. Boden, and P. Chieux, J. Non-Cryst. Solids, **150**, 80 (1992).

[8] S. Bruni, F. Cariati, A. Corrias, P. H. Gaskell, A. Lai, A. Musinu, and G. Piccaluga, J. Phys. Chem. **99**, 15229 (1995).

[9] A. Musinu and G. Piccaluga, J. Non-Cryst. Solids **192 – 193**, 32 (1995).

[10] A. Musinu, G. Piccaluga, and G. Pinna, J. Phys. Chem. **100**, 12462 (1996).

[11] C. E. Crowder, J. U. Otaigbe, M. A. Barger, R. L. Sammler, B. C. Monahan, and C. J. Quinn, J. Non-Cryst. Solids **210**, 209 (1997).

[12] L. Montagne, G. Palavit, and R. Delaval, J. Non-Cryst-Solids **215**, 1 (1997).

[13] M. G. El-Shaarawy and F. A. Radwan, J. Phys. Soc. Japan **69**, 1423 (2000).

[14] RVSSN. Ravkumar, V. R. Reddy, A. V. Chandrasekhar, B. J. Reddy, Y. P. Reddy, and P. S. Rao, J. Alloys and Compounds **337**, 272 (2002).

[15] T. M. Sabine, B. A. Hunter, W. R. Sabine, and C. J. Ball, J. Appl. Crystallogr. **31**, 47 (1998).

[16] K. Laaziri, J. L. Roberson, S. Roorda, M. Chicoine, S. Kycia, J. Wang, and S. C. Moss, J. Appl. Cryst. **32**, 322 (1999).

[17] H. H. M. Balyuzi, Acta Cryst. **A31**, 600 (1975).

[18] J. H. Hubbell, W. J. Veigele, E. A. Briggs, R. T. Brown, D. T. Cromer, and R. J. Howerton, J. Phys. Chem. Ref. Data **4**, 471 (1975).

[19] J. Krogh-Moe, Acta Crystallogr. **9**, 951 (1956).

[20] U. Hoppe, D. Ilieva, and J. Neuefeind, Z. Naturforsch. **57a**, 709 (2002).

[21] U. Hoppe, E. Metwalli, and R. K. Brow, J. Non-Cryst. Solids **297**, 263 (2002).

[22] M. Karabulut, G. K. Marasinghe, C. S. Ray, G. D. Waddill, D. E. Day, Y. S. Badyal, M.-L. Saboungi, S. Shasti, and D. Haeffner, J. Appl. Phys. **87**, 2185 (2000).

[23] D. T. Bowron, G. Bushnell-Wye, R. J. Newport, B. D. Rainford, and G. A. Saunders, J. Phys.: Condens. Matter **8**, 3337 (1996).

[24] J. M. Cole, E. R. H. van Eck, G. Mountjoy, R. Anderson, T. Brennan, G. Bushnell-Wye, R. J. Newport, and G. A. Saunders, J. Phys.: Condens. Matter **13**, 4105 (2001).

[25] D. T Cromer and J. B. Mann, Acta Cryst. **A 24**, 321 (1968).

[26] R. Kaplow, B. A. Averbach and S. L. Strong, J. Phys. Chem. Solids **25**, 1195 (1964).

[27] E. Lorch, J. de Physique **C2**, 229 (1969).

[28] K. H. Althoff, W. v. Drachenfels, A. Dreist, D. Hussmann, M. Neckenig, H. D. Nuhn, W. Schauerte, M. Schillo, F. J. Schittko, and C. Wermelskirchen, Part. Accel. **27**, 101 (1990).

[29] D. Reich, Diploma thesis, Bonn-IB-94-10 (1994).

[30] M. Lemonnier, O. Collet, C. Depautex, J. M. Esteva, and D. Raoux, Nucl. Instr. Meth. A **152**, 109 (1978).

[31] E. A. Stern, M. Newville, B. Ravel, Y. Yacoby, and D. Haskel, Physica B **208 – 209**, 117 (1995).

[32] S. I. Zabinsky, J. J. Rehr, A. L. Ankudinov, R. C. Albers, and M. J. Eller, Phys. Review B **52**, 2995 (1995).

[33] N. Zotov, In: NATO ASI Series 'Amorphous Insulators and Semiconductors', Eds. M. F. Thorpe and M. Mitkova, Plenum Press 1997, pp. 225.

[34] U. Hoppe, G. Herms, W. Gerike, and J. Sakowski, J. Phys.: Condens. Matter **8**, 8077 (1996).

[35] A. McAdam, R. H. Jost, and B. Beagley, Acta Cryst. B **24**, 1621 (1968).

[36] U. Hoppe, D. Stachel, and B. Beyer, Phys.Scripta T **57**, 122 (1995).

[37] A. Speghini, E. Soural, T. Peres, G. Pinna, M. Bettinelli, and J. A. Capobianco, Phys. Chem. Chem. Phys. **1**, 173 (1999).

[38] R. L. Mozzi and B. E. Warren, J. Appl. Cryst. **2**, 164 (1969).

[39] K. Suzuki and M. Ueno, J. de Physique C **8**, 261 (1985).

[40] L. Cervinka, J. Bergerova, and M. Trojan, J. Non-Cryst. Solids **192 – 193**, 121 (1995).

[41] D. T. Bowron, G. A. Saunders, R. J. Newport, B. D. Rainford, and H. B. Senin, Phys. Rev. B **53**, 5268 (1996).

[42] R. Anderson, T. Brennan, G. Mountjoy, R. J. Newport, and G. A. Saundres, J. Non-Cryst. Solids **234**, 286 (1998).

[43] J. M. Cole, R. J. Newport, D. T. Bowron, R. F. Pettifer, G. Mountjoy, T. Brennan, and G. A. Saunders, J. Phys.: Condensed Matter **13**, 6659 (2001).

[44] M. Karabulut, G. K. Marasinghe, E. Metwalli, A. K. Wittenauer, R. K. Brow, C. H. Booth, and D. K. Shuh, Phys. Rev. B **65**, 104206-1 (2002).

[45] Lin-Yunfei, Zhang-Yan, Huang-Weiwei, L. U. Kunquan, and Zhao-Yaqin, J. Non-Cryst. Solids **112**, 136 (1989).

[46] A. Musinu, G. Piccaluga, G. Pinna, G. Vlaic, D. Narducci, and S. Pizzini, J. Non-Cryst. Solids **136**, 198 (1991).

[47] G. K. Marasinghe, M. Karabulut, C. S. Ray, D. E. Day, M. G. Shumsky, W. B. Yelon, C. H. Booth, P. G. Allen, and D. K. Shuh, J. Non-Cryst. Solids **222**, 144 (1997).

[48] M. Bionducci, G. Licheri, A. Musinu, G. Navarra, G. Piccaluga, and G. Pinna, Z. Naturforsch. **51a**, 1209 (1996).

[49] A. Balerna, M. Bionducci, A. Falqui, G. Licheri, C. Meneghini, G. Navarra, and M. Bettinelli, J. Non-Cryst. Solids **234**, 607 (1998).

[50] E. A. Stern, Phys. Rev. B **10**, 3027 (1974).

[51] H. Otto, Z. für Krist. **63**, 222 (1926).

[52] T. Stefanidis and A. G. Nord, Acta Cryst. C **40**, 1995 (1984).

[53] D. R. Tallant, C. Nelson, and J. A. Wieder, Phys. Chem. Glasses **27**, 71 (1986).

[54] W. Bues and H.-W. Gehrke, Z. für Anorg. und Allg. Chemie **288**, 307 (1956).

[55] C. Nelson and D. R. Tallant, Phys. Chem. Glasses **26**, 119 (1985).

[56] G. B. Rouse, Jr, P. J. Miller, and W. M. Risen, Jr, J. Non-Cryst. Solids **28**, 193 (1978).

[57] B. N. Nelson and G. J. Exarhos, J. Chem. Phys. **71**, 2739 (1979).

[58] J. J. Hudgens, R. K. Brow, D. R. Tallant, and S. W. Martin, J. Non-Cryst. Solids **223**, 21 (1998).

[59] P. J. Miller, J. Chem. Phys. **71**, 997 (1979).

[60] K. Y. Leung and C. Calvo, Can. J. Chem. **50**, 2519 (1972).

[61] R. Pascard, M. Chaunac, and E. Grison, Bull. Soc. Chim. France **2**, 429 (1971).

[62] E. A. Robinson, Can. J. Chem. **41**, 3021 (1963).

[63] R. F. Bartholomew, J. Non-Cryst. Solids **7**, 221 (1972).

[64] J. R. Van Wazer, Phosphorous and its Compounds, vol. 1, Interscience, New York 1958

[65] ICSD (1999). Inorganic Crystal Structure Database, Fachinformationszentrum Karlsruhe (National Institute of Standards and Technology).

[66] Z. F. Yin, M. Kasrai, G. M. Bancroft, K. H. Tan, and X. H. Feng, Phys. Rev. B **51**, 742 (1995).

[67] J. M. Wiench, B. Tischendorf, J. U. Otaigbe, and M. Pruski, J. Mol. Struct. **602**, 145 (2002).

[68] B. C. Sales, L. A. Boatner, and J. O. Ramey, J. Non-Cryst. Solids **232 – 234**, 107 (1998).

[69] B. C. Sales, L. A. Boatner, and J. O. Ramey, J. Non-Cryst. Solids **263 – 264**, 155 (2000).

[70] J. Koo, B.-S. Bae, and H.-K. Na, J. Non-Cryst. Solids **212**, 173 (1997).